Advanced Composites and Hybrid Materials (2025) 8:349
https://doi.org/10.1007/s42114-025-01361-7

RESEARCH

A recyclable PANI/PAAMPSA nanocomposite with repeatable, rapid, autonomous self-healing, and unprecedented electro-mechanical properties

Colton Duprey[1,2] · Arya Ajeev[1] · Dajung Hong[3] · Katherine Webb[4] · Sarah Veres[5] · George Chen[5] · Emily Linn[5] · Gina Lusvardi[5] · Zhongqi Liu[6] · Ruigang Wang[6] · Sanggyu Yim[3] · Zhanhu Guo[7] · Zachary Farrell[8] · Luke A. Baldwin[9] · Yang Lu[10] · Ju-Won Jeon[3] · Evan K. Wujcik[1,2]

Received: 10 September 2024 / Revised: 21 May 2025 / Accepted: 5 June 2025

Abstract
Wearable sensors, stretchable electronics, and many soft robotic materials must have a balance of conductivity, stretchability, and robustness. Intrinsically conductive polymers offer a critical step toward improving wearable sensor materials due to their tunable conductivity, soft/compliant nature, and ability to complex with other coactive molecules (i.e., polyacids, small molecules). The addition of synergistic nanofillers has been shown to enhance the conductivity, self-healing, and mechanical properties of the polymers for soft robotics and wearable applications. The development of a robust polymer nanocomposite material that offers ultra-stretchability, an autonomous self-healing ability, and enhanced electronic properties has long eluded researchers. Herein, we show an aqueous polyaniline [PANI]:poly(2-acrylamido-2-methylpropane sulfonic acid) [PAAMPSA]:phytic acid [PA] polymer complex synthesized with 0.5 wt % silver nanowires (AgNW) to form a polymer nanocomposite with high electronic sensitivity, unique mechanical properties (a maximum strain of 4693%) and repeatable/autonomous self-healing efficiencies of greater than 98%. This AgNW polymer complex has an engineering strain higher than any reported hydrogel or other polymer-based sensor materials, in which the interface between the polymer matrix and the AgNW is hypothesized to be integral for the formation of the active electrically conductive network and unprecedented mechanical properties. To illustrate the remarkable sensitivity, the material was employed as a biomedical sensor (pulse, voice recognition, motion), topographical sensor, and high-sensitivity strain gauge.

Keywords Repeatable self-healing · Polymer electronics · Ultra-stretchable · Wearable sensors · Extreme mechanical properties

1 Introduction

Polymer nanocomposites (PNCs) have been utilized in a number of applied areas including environmental engineering [1, 2], aerospace [3–5], energy storage [6–8], and biomedical monitoring [9, 10]. As bio-monitoring and wearable sensors have become a large area of interest, a definite need for wearable sensors that are flexible or stretchable, soft, and highly electrically conductive has emerged [11–14]. Typical inorganic electronic sensors are rigid and brittle, and the skin-inspired polymer electronics which allow wearers more flexibility and comfort, unfortunately, have issues with sensitivity as well as stability over time [9, 10]. For a polymeric material to be used in a wearable sensor, it must possess comparable properties to the skin in terms of stretchability and elasticity. Self-healing is a highly beneficial attribute of biological systems. It allows them to autonomously repair materials in the event of mechanical damage, and this attribute is desirable in conductive polymers which will be used as wearable sensors. Polyaniline (PANI) is a well-studied conductive polymer which has acquired great interest due to its high conductivity as a result of its conjugated backbone; yielding itself to potential usage in electronics [15–17]. A conductive polyaniline (PANI)-based polymer complex with high stretchability and elasticity comparable to human skin, and autonomous, repeatable self-healing properties was developed previously [15, 18]. The investigated polymer composite is composed of PANI, a small molecule dopant [phytic acid (PA)], and a polyelectrolyte [poly(2-acrylamido-2-methylpropane sulfonic acid)

Extended author information available on the last page of the article

Published online: 05 September 2025

(PAAMPSA)]) [15]. PAAMPSA is a hygroscopic polymer electrolyte with a deprotonated sulfonic acid group. It is used to not only template the oxidative polymerization of aniline to form PANI but also to help utilize its electrolytic counterions to facilitate electron transport and increase conductivity. PA is a small molecule acid with six dihydrogen phosphate groups. The PA acts as both a P-type dopant to form the emeraldine salt form of PANI and a non-covalent crosslinker for the polymer matrix. The sulfonic acid and phosphate groups in the polymer complex allowed for copious hydrogen bonding and electrostatic interaction which yielded impressive mechanical properties, and the conductivity of the material measured to be 2 S/m [15].

To further increase the conductivity of the material and by extension its sensitivity, silver nanowires (AgNWs) were added to the polymer complex as a filler for their high conductivity (6.3×10^7 S/m) and larger surface area compared to other nanowires [19, 20]. The addition of metallic nanofillers into polymeric piezoresistive sensors to increase sensitivity is well-studied. In systems where cracking occurs in the polymeric matrix throughout stretching and movement, or where fractures initially occur, the highly conductive nanofiller can bridge separated conductive pathways, allowing for the preservation of conductivity in the material as a whole [21]. One example of the utilization of this bridging phenomenon showed the sensitivity of polyurethane to increase by over fifteen times with the addition of multi-walled carbon nanotubes (MWCNTs), with their bridging also allowing for an increase in the system's strain sensing range [22]. In cases where the nanofillers are supported by or contained in a material that can maintain a conductive pathway the separation of the nanofillers, or the formation of microcracks, can lead to very high sensitivities as a result of the more conductive metallic pathways breaking [23]. AgNWs are a flexible cylindrical rod shape with a face-centered cubic (FCC) structure [24]. The FCC lattice is a closely packed cubic structure. Since there are more atoms in individual FCC crystal cells than in other cubic cells, stresses are easily accommodated and more evenly distributed [25]. This superior stress management allows the material to maintain its high stretchability and flexibility under mechanical stresses and strains. Distributing AgNWs into the polymer matrix produces a conductive yet flexible material due to the high intrinsic flexibility of AgNWs that arises from their high average aspect ratio of 1250 [26]. In this electrically conductive nanowire-based nanocomposite, the interface between the matrix and the AgNW is integral for the formation of an active conductive network [24].

The addition of metallic nanofillers into polymeric systems typically increases conductivity in accordance with percolation theory, forming connected pathways of these high-conductivity materials within the polymer matrix, thus creating a path of least resistance for electrons to flow, increasing the conductivity of the composite material. Additionally, the high aspect ratio of nanowires forms an interconnected electrically conductive network even at low volume fractions. However, the introduction of these non-stretchable, more brittle elements into the soft and compliant network often interrupts the polymer matrix, with the potential to decrease mechanical properties. While it was initially hypothesized that the AgNWs would increase the conductivity and decrease the mechanical properties of the polymer complex, the AgNW/PNC's mechanical performance increased drastically. Based off of prior studies, nanoparticles and other nanomaterials typically improve self-healing ability in polymeric systems with extrinsic self-healing properties [27–29], but are unlikely to improve the self-healing efficiencies of an intrinsically self-healing polymer.

Self-healing is a highly beneficial and desirable attribute of biological systems that allows them to autonomously repair materials in the event of physical damage. Recently, flexible/stretchable electronics and wearable sensor researchers have been motivated to imitate this behavior in innovative devices with unique and unprecedented electro-mechanical properties. Conductive self-healing polymers have been used to improve a range of electronic and optoelectronics devices, including wearable sensors and displays for healthcare [9, 10, 30], virtual reality [31], and soft robotics [32], among many others [18, 33, 34]. There are various physical and chemical methods utilized in creating self-healing materials such as containing a healing agent in microcapsules, chemically integrating dynamic reversible bonds, and self-repairing through intrinsic means [35, 36]. Self-healing routes are typically divided into extrinsic or intrinsic, and then further subdivided into autonomic or non-autonomic [37–39]. Non-autonomic self-healing polymers require the use of an external trigger, such as heat, light, or force [37]. Conversely, the damage to the polymer is the only trigger needed for an autonomic self-healing complex [37]. Self-repair through autonomic means can occur via Van der Waals interactions or through electrostatic forces and hydrogen bonding. These methods have been explored recently [40–42] and provide advantages over the other methods due to the fact that they are autonomous and repeatable [28]. Van der Waal interactions occur due to their high polarity, and hydrogen bonding works because of the dipole—dipole interactions between hydrogen atoms and carbon, nitrogen, or oxygen atoms [43, 44]. In many systems, this autonomous self-healing capability is attributed to the dynamic supramolecular hydrogen bonds and intramolecular interactions among the polymer chain [45]. This type of self-healing is the most desirable since healing has few requisites and is repeatable and fully autonomous, thus improving the longevity and reuse of the material. A self-healing polymer complex with dynamic reversible bonds has been synthesized at room temperature with excellent mechanical properties;

however, in many cases, hours are needed after deformation to regain nearly 100% of the original mechanical properties [46]. Intrinsic self-healing possesses a latent healing ability that is triggered by damage to the polymer and does not require the use of a catalyst [39]. While intrinsic self-healing is appealing because the cross-linking can be rebuilt repeatedly, the self-healing mechanisms typically involve covalent bonding and therefore often require some form of external stimuli such as heat or light to carry out the reaction. Alternatively, extrinsic self-healing often requires the dispersion of micro-encapsulated catalysts which, when damaged and released, initiate reactions to reconstruct the cross-linking networks within the polymer [38]. A major roadblock with utilizing healing agents is the issue of lack of repeatability or the "one-and-done" usage [36]. The chemically integrated dynamic reversible bonds are often based on temperature and typically either have poor mechanical properties or will only be able to mend tears and dents at higher temperatures [36]. The drawback of this method is that the polymer has a limited number of cycles it can be self-healed and often cannot self-heal in the same location repeatedly.

Recently, Lu et al. [15] have developed an ultra-stretchable PANI-based polymer complex with a repeatable near-instantaneous autonomous self-healing ability that has overcome many of the hurdles commonly seen in self-healing electronic polymer materials. However, further improvement of conductivity and electronic sensitivity is desirable for wearable applications, i.e., to accurately detect slight changes in movement or pressure. To accomplish this, silver nanowires (AgNWs) were added and dispersed throughout the developed polymer complex to increase its mixed-ionic-electronic sensitivity. The investigated polymer composite is composed of PANI, a small molecule dopant [phytic acid (PA)], a polyelectrolyte [poly(2-acrylamido-2-methylpropane sulfonic acid) (PAAMPSA)], and AgNWs (Scheme Fig. 1). PAAMPSA is a hygroscopic polymer electrolyte with a deprotonated sulfonic acid group. PA is a small molecule acid with six dihydrogen phosphate groups. PANI polymer has acquired great interest recently due to its high conductivity and potential use in electronics [15–17]. To illustrate the applicability of these materials, developed biomedical, high-sensitivity pressure, and topographical monitoring devices are employed. These detection schemes require materials with the ability to act as natural skin and would include adequate properties of compliancy, elasticity, omnidirectional stretching, and the added ability to repeatedly and autonomously self-heal [15]. In addition to these mechanical properties, other electrical properties are necessary to ascertain an accurate piezoresistive strain sensor, that can be used in applications such as soft robotics or wearable biomechanical sensors.

2 Results and Discussion

The AgNW/PNC film was prepared via a simple three-step method previously demonstrated in Fig. 1. The first step is an *in-situ* oxidative polymerization of aniline utilizing ammonium persulfate (APS) as an initiator. The APS initiates the polymerization of aniline by oxidizing it to the emeraldine form. Then in the presence of the phytic acid, the doped emeraldine salt form, the most electrically conductive form of polyaniline, is produced as the solution turns a dark green color [47, 48]. The reaction occurs via a type 1 (also known as zip) templated polymerization with the PAAMPSA acting as the templating molecule, which helps guide polyaniline into straighter molecular chains held in place by electrostatic interactions and hydrogen bonding with the sulfonic acid groups of the PAAMPSA. After the polymerization of the aniline is completed, the AgNWs are dispersed throughout the polymer complex solution. It is imperative that the AgNWs are added post-polymerization so they are not oxidized by the APS, which would decrease their mechanical performance as well as their conductivity. After sonication

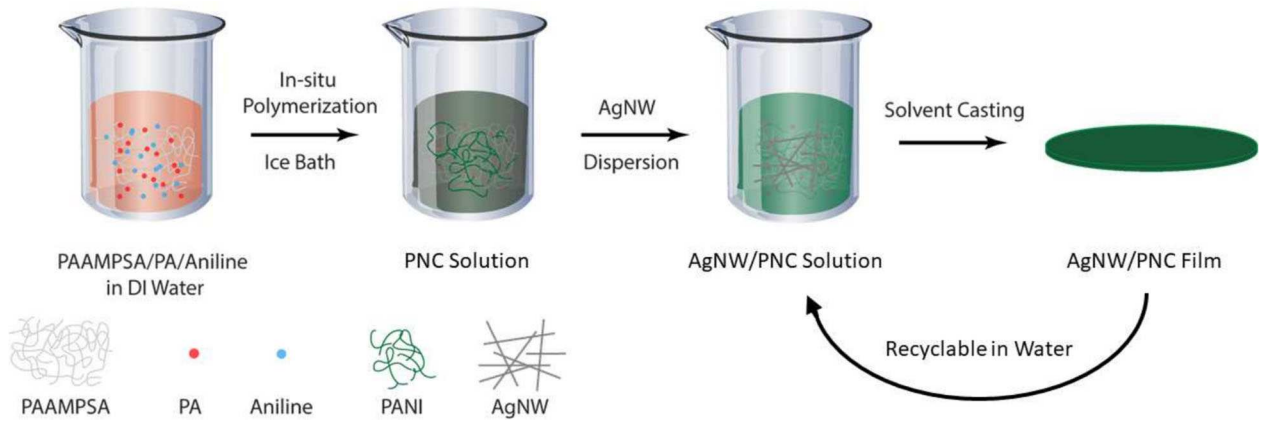

Fig. 1 Schematic illustration showing the simple, aqueous, and scalable synthesis of AgNW/PNC films

and stirring to ensure homogeneity and minimize the potential agglomeration of the AgNWs, the solution is solvent casted in a Teflon petri dish where excess water evaporates. The color change from clear to green as the aniline rearranges to the emeraldine salt form indicates that the synthesis for the polymerization was complete. The p-type doping of PANI utilizing a protic acid increases the crosslinking as well as the electrical conductivity of PANI [16, 49, 50]. The unique doping pathways to the emeraldine salt of PANI occur through either charge-transfer or protonation [49], making Lewis acids such as PA ideal candidates for p-type doping of polyaniline. PA has been shown to increase PANI's electrical and mechanical properties due to an increase in the cross-linking [51]. It has been shown that polymer acids can be used as dopants to stabilize the electrical states of the polymers [49]. In this case, PA and PAAMPSA act as protonation agents for doping PANI which aids the cross-linking of both hydrogen bonding and PANI chains [49, 52]. This, in turn, creates a deprotonated polyelectrolyte, an anion, and a doped conductive polymer that possesses self-healing properties due to the cross-linking of hydrogen bonds and intramolecular electrostatic interactions [15]. Not only is PA an efficient doping agent for PANI, it is also beneficial in terms of water dispersibility, allowing for the polymer composite to be synthesized with water as the only solvent [15, 52, 53]. This is important from an industrial perspective as solubility in common solvents is highly favorable [53]. Aqueous processing has the added benefit of being considered a green and highly renewable process. While many organic electronic materials are synthesized using multiple organic solvents [54–56], our developed synthesis is both sustainable and scalable. The water solubility of the complex also allows for the AgNW/PNC to be easily recyclable, as it can be dissolved in water and solvent casted again as illustrated in Fig. 1.

The morphology of the AgNW/PNC was observed by SEM and can be seen in Fig. 2. The AgNWs used in our nanocomposite have a uniform size with an average diameter of 20 nm (Fig. 2a). The surface of the AgNW/PNC film was microscopically smooth and flat (Fig. 2b), with only a few nanowires being visible. Thanks to the high viscosity of AgNW/PNC suspension, the AgNWs are uniformly dispersed in the AgNW/PNC nanocomposite; an auspicious indicator that edge effects and the casting process did not cause the AgNWs to come to the surface of the material or agglomerate. The nanowires can be seen as the numerous white dots in Fig. 2c. The EDS elemental mapping in Fig. 2d, e confirms that the white dots are the AgNWs. In the cross-section view of Fig. 2c, we see wrinkles indicated by the orange arrows, likely a result of the casting process occurring layer by layer as the kinetics of phase separation and phase change are dynamically altering during the entire film formation process [57]. Some important effects include thermal gradients near the liquid–vapor and liquid–solid interfaces, the evaporation rates, and the concentration-dependent mobilities. The orange dashed circles depict some AgNWs protruding above the cross-section which have close-to-parallel angles between the nanowires

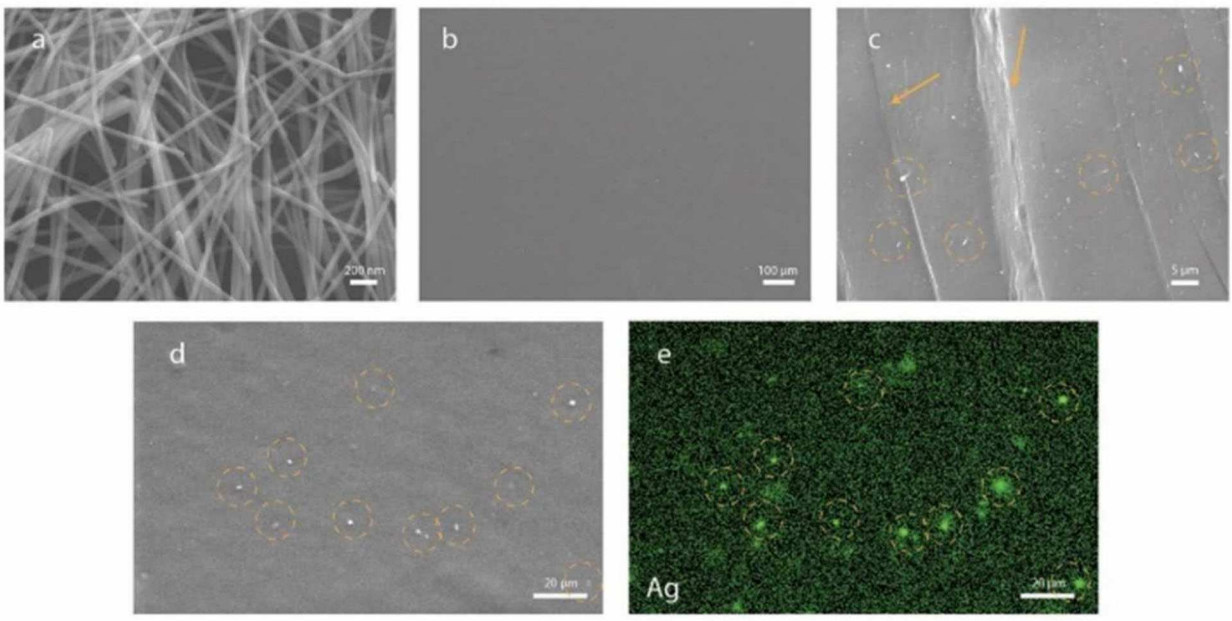

Fig. 2 SEM images of AgNW/PNC. **a** The silver nanowires. **b** The surface of AgNW/PNC. **c** Cross-sectional SEM image of AgNW/PNC. **d**, **e** EDS mapping of Ag element on cross-section of AgNW/PNC

and the cross-section; indicative of some sort of interfacial interaction with the AgNWs and the material. This is important to note as the interfacial adhesion between AgNWs and the PNC can affect the electrostatic interactions as well the electron movement as it pertains to conductivity [58]. EDX data of the neat AgNWs can also be seen in S11 in the SI.

The XPS data collected (Fig. S3, Table S1) confirms that there are PAAMPSA, PANI, PA, and AgNWs in the polymer complex. The N1s peak at 398 eV indicates that there is an NH group in the polymer complex, and with N^{+}, and N^{2+}. The peaks at 165.91 eV and 131.91 eV correspond to the deprotonated sulfuric acid groups in PAAMPSA, and the phosphoric acid groups in phytic acid, respectively. The N1S peak corresponds to NH and N^{+} and N^{2+} respectively. The large peak at around 365.91 eV shows the Ag3d in the AgNW/PNC.

While there was concern that the AgNWs may inhibit the dynamic hydrogen bonding between the PAAMPSA, PANI, and PA, the excellent autonomous self-healing ability of the polymer complex is well-preserved with the addition of the AgNW percolation network. The self-healing properties of the AgNW/PNC complex were tested according to the procedure discussed in previous work [15]. The AgNW/PNc polymer complex showed similar self-healing efficiencies. When cut and placed back together, the complex takes approximately 3 h to recover its conductivity, and demonstrates repeatable conductive healing over multiple cycles. While it has previously been discussed that the PNC sensor's autonomous self-healing ability is a result of dynamic hydrogen bonding, the AgNWs appear to contribute. This is likely as a result of the readily available electrons of silver interacting with the positively charged holes in the doped polyaniline. These opposite forces attract one another, allowing the polymer matrix to tightly bind to the surface of the AgNWs again after self-healing. With the stretchability of composite materials being so closely related to cohesion between the matrix and filler, [59] this interaction between the AgNWs and polymer matrix is imperative to recover mechanical properties after self-healing. If this interfacial adhesion didn't occur, voids between the AgNWs and polymer matrix would form, causing losses in both conductivity and mechanical properties. Figure 3 shows the representative optical images of self-healed AgNW/PNC film after being cut in half. Note that the AgNW/PNC film has an appearance of dark green color (Fig. 3a), a characteristic result of the polyaniline existing in its doped emeraldine salt form. At the incident angle of reflection, the film looks shiny (Fig. 3b) which enables us to observe the self-healing phenomena more easily. The initial

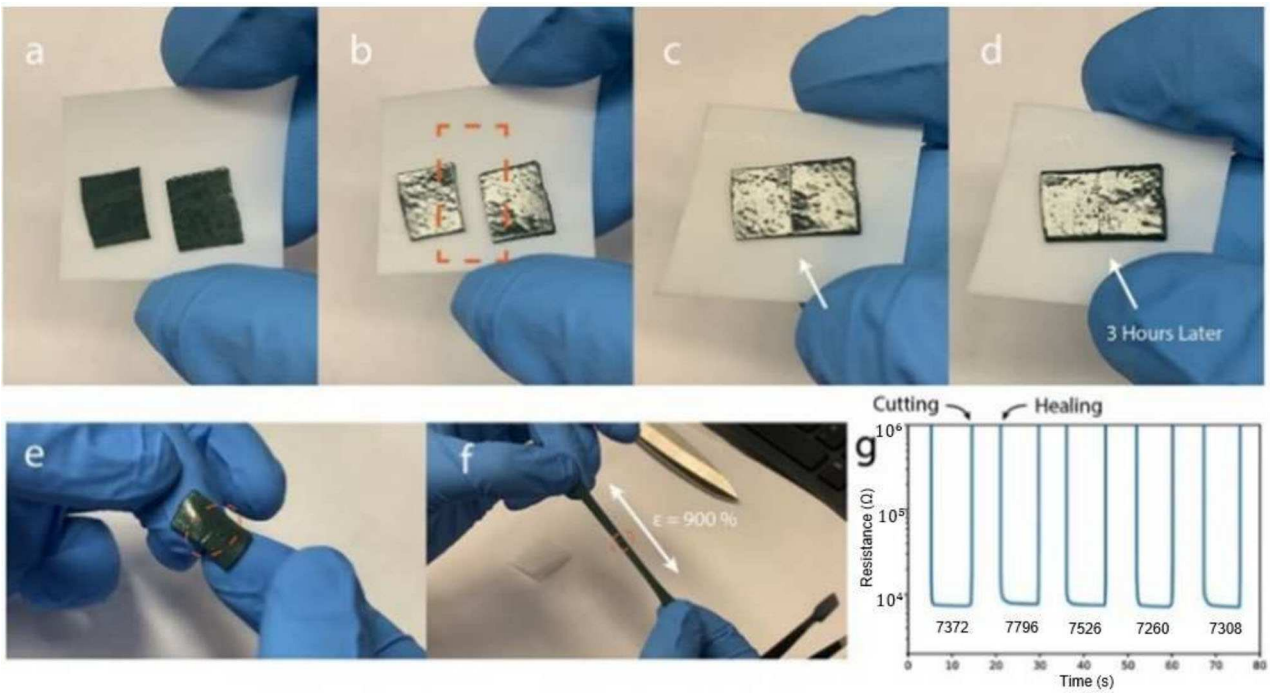

Fig. 3 Optical images of AgNW/PNC film after being cut in half. **a** The severed film of the characteristic green-colored PANI in its emeraldine salt (highly electrically conductive) form. **b** The shine of the film allows us to easily view the interface where the sample was cut. The severed sides are highlighted by dashed lines. **c** The two severed surfaces were gently placed in contact with one another to begin the autonomous self-healing process. **d** The autonomously healed film after 3 h. **e**, **f** The healed film can be stretched up to 900% strain without rupturing. **g** The monitored resistance changes for 5 cut-heal cycles of AgNW/PNC film at the same location. The value beneath the line was the average resistance during a 5-s healing window

AgNW/PNC sample was cut with scissors into two severed portions. The detached surfaces of these were placed in contact with each other to begin the autonomous self-healing process. After 3 h, without any external stimuli (force, light, heat, etc.), the two halves of the film had self-healed into one and the visible interface at which the sample had been fractured disappeared. The self-healing performance was further studied in terms of mechanical and electrical properties. Figure 3e, f shows that the self-healed film can be stretched to 900% strain by hand without rupturing. If pressure is applied by hand to reconnect the severed pieces of the AgNW/PNC complex, the electrical conductivity of the AgNW/PNC is almost entirely restored 3 s after the severed pieces are connected. This was tested for five cycles, demonstrating an excellent repetitive electronic self-healing ability; with >98% of the original electrical conductivity being restored within those first 3 s. While the autonomous and intrinsic self-healing of the AgNW/PNc is impressive, its similarity to previous work merits less of an investigation [15], as the extreme increase in stretchability as well as the increase in sensitivity appear to be more enlightening with regards to how the added AgNWs are functioning within the polymer complex.

While the increased sensitivity of the polymer complex with the addition of the AgNWs is substantial and likely related to the production of interconnected electrically conductive pathways of AgNWs within the sensor, the increase in mechanical properties remains somewhat enigmatic. In order to investigate the interfacial interactions between the AgNWs and the polymer complex, a rheometric study was conducted; the results of which are shown in Fig. 4. Initially, the study was conducted between a neat polymer complex sample as seen in the previous work [15], and the AgNW/PNC sample. Once that initial study concluded that the rheology of the two samples was significantly different, it was hypothesized that the difference in mechanical performance must lie in the interfacial interactions between the AgNWs and the polymer complex. As a result, an investigation was done comparing the AgNW sample to one with silicon carbide nanowires (SiCNWs, seen in Fig. 4a). SiCNWs are very chemically

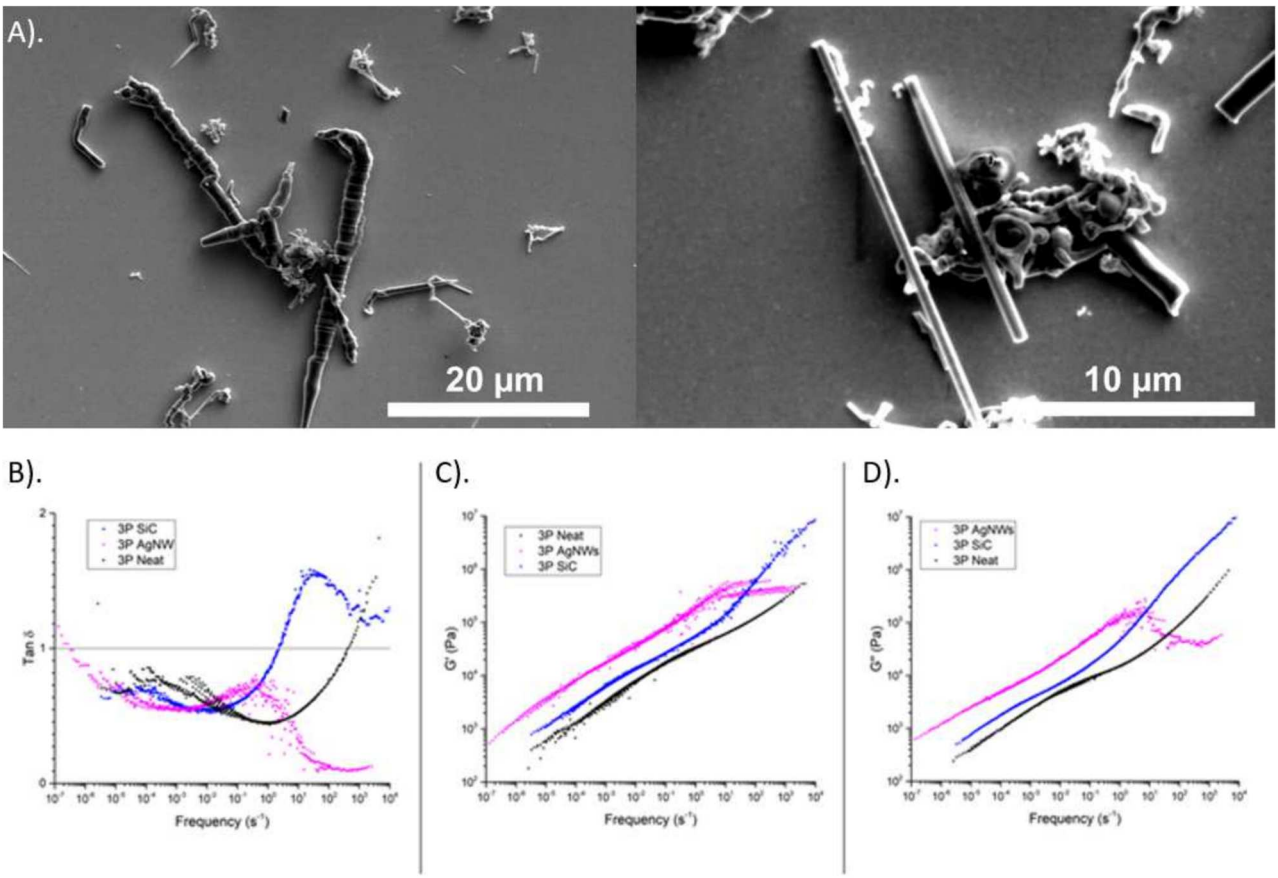

Fig. 4 **a** SEM micrograph of silicon carbide nanowires (SiCNWs) before (left) and after (right) etching using hydrofluoric acid, a process utilized to remove oxidized layers from the surface of nanomaterials. Rheological data showing the **b** storage modulus (G′), **c** loss modulus (G″), and **d** damping factor ($\tan\delta = \frac{G''}{G'}$) for the neat polymer complex, AgNW/PNC, and the SiCNW/PNC

resistive and thermally stable [60, 61]. They were selected to confirm that interfacial interactions took place between the AgNWs and the polymer complex, as they are nonreactive in both acidic and basic conditions [62], and therefore should not have interfacial reactions with the PNC complex. The three samples were run utilizing a parallel-plate configuration rheometer as the storage modulus (G′), loss modulus (G″), and damping factor ($\tan\delta = \frac{G''}{G'}$), were measured versus frequency, and can be seen in Fig. 4b–d. The storage modulus or G′ vs frequency graph indicates that all three of the materials stiffen at higher frequencies, meaning that the material begins to behave as a viscous liquid, with the hydrogen bonding and self-healing effects inducing less elasticity. However, it is important to note that the AgNW sample appears to hit an asymptote, where the frequency no longer causes the storage modulus to increase. This asymptote, where the solid-like behavior of the AgNW sample occurs at a frequency of 10 Hz, represents a point where the material's ability to store energy elastically levels off. Most likely due to the hydrogen bonding of the polymeric chains being unable to provide elasticity at the rate at which the shear stress is being applied. It is important to note that before this point the storage modulus for the AgNW sample is greater than that of the other two, meaning it is more elastic and has more interfacial adhesion, indicating a greater degree of non-covalent cross-linking being present in the material [63]. This broadening of relaxation modes that occurs in the AgNW sample is typically indicative of the chain-pinning phenomenon taking place. The AgNWs within the sample pin polymer chains into one another, helping to increase entanglements and thus their electrostatic interactions between one another. This phenomenon can increase the elasticity of materials and is likely the cause of the increase in stretchability seen in the mechanical testing in Fig. 5. The damping factor, describing the ratio of the two viscoelastic quantities, increases somewhat linearly for the neat polymer and SiCNW/PNC samples; however, the AgNW/PNC sample increases to a point and then once again levels off and stops changing. The asymptote of the damping factor correlates to the liquid-like behavior of the AgNW/PNC stabilizing and becoming constant, which could indicate that the sample has relaxed and rearranged to accommodate the strain being applied so frequently. This ability of the material to rearrange via dynamic hydrogen bonding is shown in the SiCNW/PNC sample as well but is significantly higher

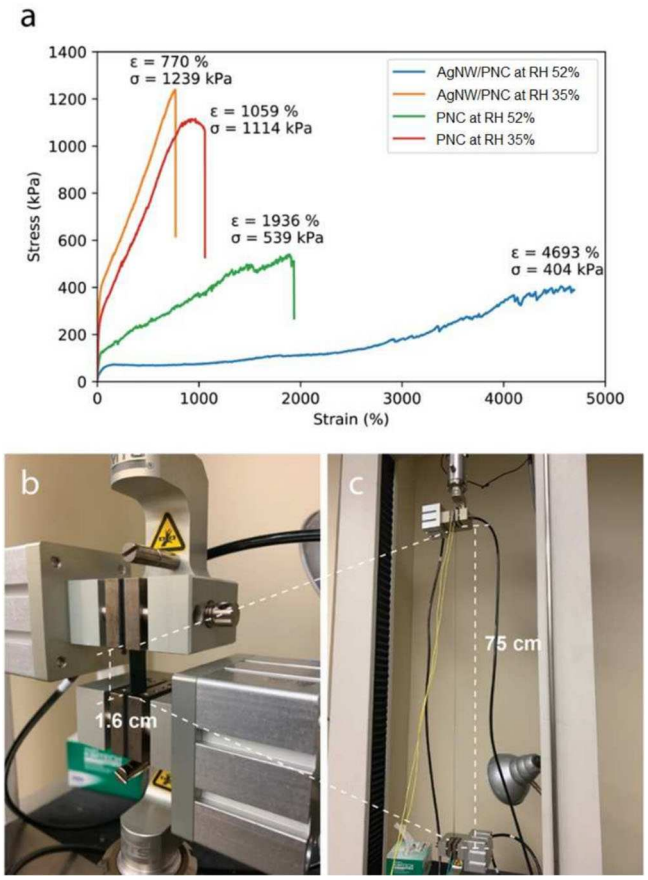

Fig. 5 Mechanical testing and the results from mechanical testing. **a** Tensile strain–stress curves for AgNW/PNC and polymer complex films. **b**, **c** Photographs demonstrating the ultra-high stretchability of the AgNW/PNC nanocomposite (~ 47×)

in the AgNW/PNC. These two samples demonstrating this ability support the theory of a chain-pinning phenomenon occurring in the material, where the nanowires (both AgNW and SiC) are penetrating multiple polymer chains. This chain pinning increases entanglements among the polymers in the material, thus making the material more stretchable. Since the ability of the polymer matrix to transfer stress to the filler is an important indicator of tensile strength in a composite material, it is imperative that the interfacial adhesion of the polymer matrix and fiber in a composite material are strong [59, 64]. This interfacial strength at the polymer-nanofiber boundary can help to decrease porosity within the material as it begins to stretch [65]. The increase in porosity of a composite material, particularly the porosity between the filler and polymer matrix has been shown to decrease the tensile strength of said composite [66–68]. As the material stretches, the localized shear strain of atoms at the interface with the reinforcing filler is less than those further away, meaning that the polymer matrix can maintain a more consistent density by adhering to the nanofillers, allowing tensile force to be applied over a more uniform area and increasing the ultimate tensile strength [59, 69]. One thing that likely increases the interfacial adhesion between the PNC matrix and AgNWs is that the AgNWs have a polyvinylpyrrolidone (PVP) capping agent that is left over at the end of their synthesis (approximately 0.5 wt%). Since the AgNWs have a pentagonal structure, it is known that the chain length of the PVP is likely to be a minimum of just under 40,000 repeat units [70]. Our PAAMPSA molecules have an average chain length of approximately 3900 repeat units, meaning that the introduction of this long-chain polymer could help reinforce the interface and provide entanglement with the polymer matrix [71]. The OH groups of the AgNWs also contribute to the dynamic hydrogen bonding throughout the PNC/AgNW complex.

The AgNW/PNC exhibits an impressive ultra-high stretchability of at least 4693%, as demonstrated in Fig. 5. /hlThe 0.9 mm thick solution cast film with a gauge length of 1.6 cm was stretched to 75 cm before breaking. The elongation at break is at or above 4963%, where the testing limit of the tensile tester was reached. With regards to self-healing, the polymer complex undergoes enough irreversible plastic deformation at just under 2000% strain, where a very slight peak can be seen in Fig. 5a. At this strain, the polymer complex undergoes significant necking as the polymer chains and AgNWs reorganize. As a result, the self-healing mechanism sees a significant reduction in its effectiveness, as the interface of the polymer complex at the breaking point will be thinner and therefore have less surface area to self-heal at. Above this strain, the polymer complex may adhere to itself still; however, the mechanical and electrical properties will not return to their original states, and therefore, the complex loses its self-healing ability. With regard to the maximum recoverable tensile limit, it can be hard to measure in such a dynamic material. Since the rheometric study supports the hypothesis that the material is rearranging to accommodate stress, the stress doesn't change as much relative to the strain being applied. Due to the large plateau as the tensile tester operates and stretches the material, and the linearity of that range relative to the beginning of the test, the maximum recoverable tensile limit of the AgNW/PNC material should be 85 kPa. Something important to note, however, is that while this limit represents where plastic deformation begins to occur, it is not the limit of the material breaking, but rather where the material begins to relax in order to accommodate this stress. In comparison, a recent review of academic strain sensors found that recently developed strain sensors have a stretchability from 2 to 1400% [72]. The majority of sensors found were under 600% [73–77]. Hydrogel-based strain sensors are known to have an exceedingly high stretchability, but it is uncommon to see electronic hydrogels possessing an elongation at break over 2000%. In addition, they normally contain upwards of 80 wt% water, making them environmentally unstable. The AgNW/PNC system, however, is only roughly 6–8% water based on TGA/DSC, depending on ambient humidity [15]. While many hydrogels rely on water to garner mechanical properties as well as facilitate ion transport to aid in electrical conductivity, the AgNW/PNC system needs significantly less water, allowing it to maintain relevant mechanical and electrical performance in a wider range of humidities and temperatures, affording the complex potential in a broader range of applications. The mechanical properties of the AgNW/PNC are still highly dependent on relative humidity (RH). While under ambient conditions ($\sim$ 52% RH), the stretchability of AgNW/PNC is over 4693%. This is the highest stretchability for a polymer strain sensor to date, to the best of the author's knowledge. However, the stretchability dramatically decreases to 770% (still above most reported strain sensors) under a low humidity condition (35% RH), corresponding to an 83.6% drop. The ultimate strength, however, increases from 404 to 1239 kPa with the decrease in humidity.

This hardening or softening of the material with the change in humidity and the subsequent change in mechanical performance is related to the water retention of the film. The three components of the polymer complex network form a solid polymer electrolyte via their protonation (PANI) and deprotonation (PAAMPSA, PA). It is well known that the mechanical properties of a polymer electrolyte differ significantly between a humid or dry atmosphere. The retained water promotes proton dissociation which leads to the plasticizing of the film [78]. The inference is that at higher relative humidity conditions, the mechanical properties of the AgNW/PNC composite increase alongside the conductivity as a result of the increased water available in the system that can aid in the transport of ions. As for the pure polymer

complex, the effect of plasticizing by water is less significant. These effects are best illustrated by how the mechanical properties of these polymers change due to humidity. While the polymer complex without AgNWs has a slightly larger stretchability of 1059% at a lower humidity, the AgNW/PNC has a much higher stretchability at 52% RH—twice as high as the neat polymer complex. The Young's modulus for the AgNW/PNC material is 86 kPa (c.f., 20–100 kPa for human dorsal forearm and palm[79]) which indicates that the material is extremely compliant and soft—suitable for soft robotics and wearable applications. This was initially unexpected, as the addition of these crystalline nanowires was expected to interrupt the polymer matrix and decrease the mechanical properties. However, upon a deeper review of literature, there have been many cases of polymer adsorption to additives within composite materials, causing an increase in mechanical properties [80–84]. The PAAMPSA's sulfonic acid group is likely adsorbing well to the AgNWs, which not only dissipates van der Waal forces which would otherwise cause agglomeration among the AgNWs [85], but also increases the intermolecular forces in the system, thus leading to the improved mechanical properties. The concentration of silver nanowires also had an effect on the stretchability and mechanical performance of the AgNW/PNC. At concentrations well below the optimal loading percent of 0.5 wt% AgNWs, no change between the AgNW/PNC and PNC was noticed, and as that loading increased up to 0.5 wt%, both the stretchability and sensitivity would increase, which has also been demonstrated with the usage of metallic nanofillers in other piezoresistive strain sensors [86]. Beyond 0.5 wt% AgNWs, the additional amount of crystalline AgNWs in the PNC would interrupt the polymer matrix and make the material less stretchable. Much further beyond 0.5%, and the AgNWs would begin to agglomerate, causing massive defects. At very high loading percentages the solution would form a powdery material after solvent casting.

As AgNWs are added to a polymer complex, its structure is changed to increase the number of junctions, and the number of conductive pathways of the PNC is increased [87]. This explains the increase in electrical conductivity from 1.1 to 2.1 S/m; however, the increase in mechanical properties upon the addition of the AgNWs into the polymer complex may be less intuitive. The increase in conductive paths due to AgNWs is hypothesized to allow the polymer's ability to non-covalently crosslink to be more dependent on its local environment, specifically for factors that increase the speed of electron charge carriers. The increase in humidity is able to increase the speed in which charge carriers move, hence, increasing the electrostatic properties of the AgNW/PNC, resulting in access to higher GFs [51, 88–90]. The large gauge factor is not due to the high conductivity of the material and instead occurs due to the high strain sensitivity of the polymer. This increase in sensitivity could be due to changes in the polymer matrix, specifically, the polymer surface becoming less planar and impacting interfacial adhesion as the polymer stretches [51]. The interfacial adhesion of the AgNW/PNC is thought to also be dependent on differing humidity levels, shown previously in epoxies and other polymers [91].

The electro-mechanical responses of AgNW/PNC and polymer complex to the tensile deformation are shown in Fig. 5a. The relative resistance (RR) change is defined in (Eq. 1), where R_0 is the resistance at 0% strain, and ΔR is the difference between the resistance under strain (ϵ) and R_0.

$$RR = \left(\frac{\Delta R}{R_0}\right) \times 100\% \tag{1}$$

For the neat polymer complex, the maximum relative resistance change is 21,000%. Meanwhile, the maximum relative resistance change of AgNW/PNC is a dramatic 298,000%, which is 2980 fold of its initial resistance and 14.2 fold of the maximum relative resistance change of polymer complex. While the AgNW/PNC will show a smaller change in resistance at any given strain relative to the neat polymer complex due to its lower resistivity, an increasing strain will induce a faster rate of resistance changing for both materials. To evaluate the performance of the strain sensor, the simplest metric is the gauge factor (GF). Gauge factor describes the relationship of relative resistance change and applied strain by Eq. 2, where $\Delta R/R_0$ is the relative resistance change and ϵ is the applied strain.

$$GF = \left(\frac{\Delta R/R_0}{\epsilon}\right) \tag{2}$$

It is rare to see gauge factor over 10 for electronic materials with ultrahigh stretchability ($\epsilon_{MAX} > 1000\%$) as most highly stretchable strain sensors have GF around 0.1 to 5. High gauge factors over 10 are commonly seen in brittle or poorly stretchable conductive materials[92], which will fail to work in situations when large deformation monitoring is required. The AgNW/PNC shows an extraordinarily high gauge factor of 63.3 at a strain of 4693% (Fig. 6b). The increase in gauge factor of the AgNW/PNC strain sensor corresponding to applied strains is not as prominent as the increase in relative resistance corresponding to similar strains. A comprehensive comparison of innovative strain sensors in terms of stretchability and gauge factor can be viewed in Fig. 6c. The other polymer data (Table S2) indicates that it is unusual to have a high gauge factor and a high strain simultaneously. The majority of the gauge factors recorded are under a strain of 1000%. The two sensors that have a gauge factor higher than the AgNW/PNC also had their gauge factor calculated at a strain under 500%, indicating that our polymer has a higher sensitivity than most other polymers and that it main-

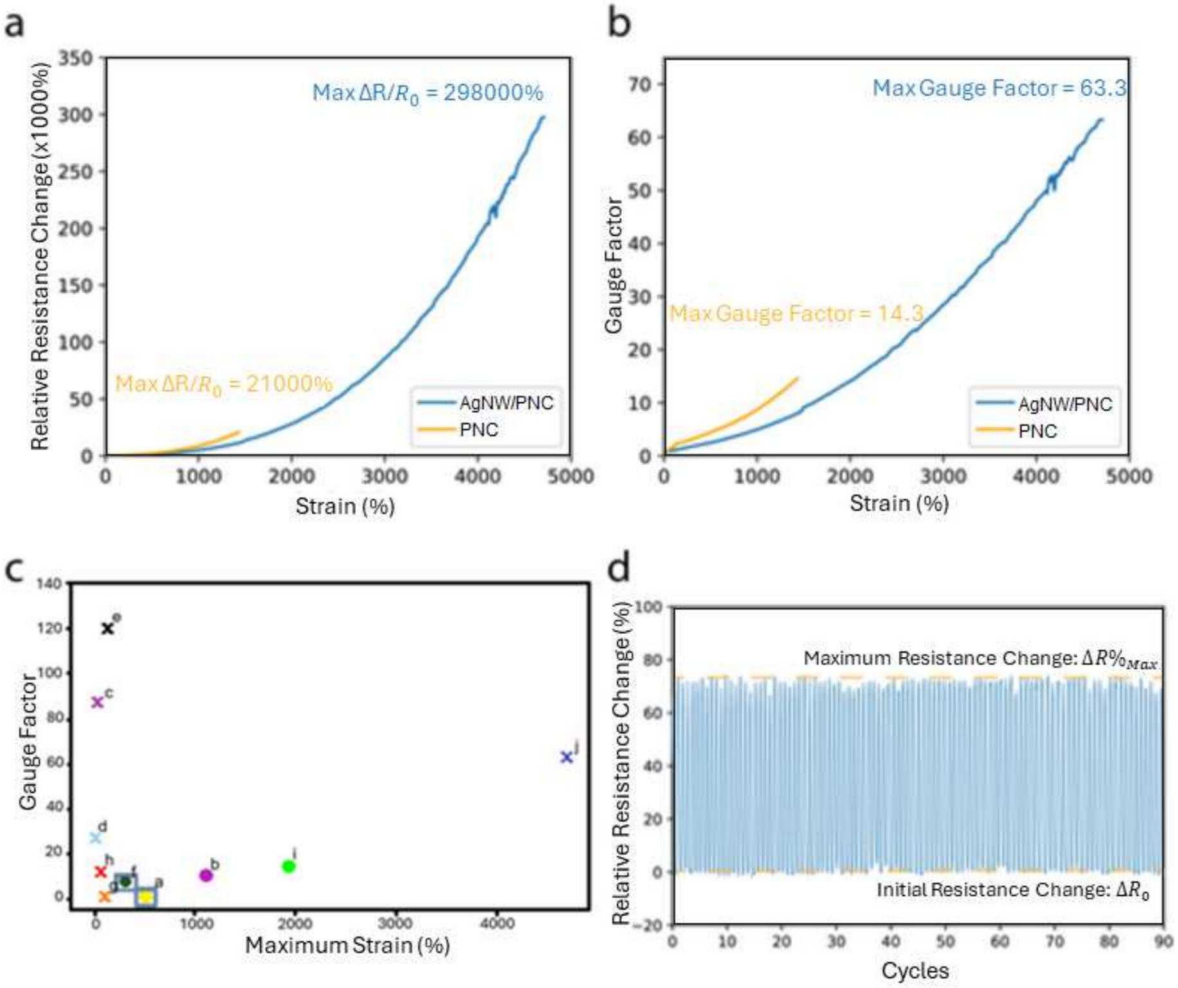

Fig. 6 Gauge factor, and relative resistance change. **a** Monitored relative resistance change and **b** gauge factor as a function of applied tensile strain for AgNW/PNC and polymer complex. **c** Comparison of recent reported piezoresistive materials with the AgNW/PNC in this study in terms of GF and maximum strain where "x" represents materials with AgNWs and "•" represents materials without AgNWs, the square represents materials that are not repeatedly self-healing [refs: a [98], b [97], c [96], d [95], e [94], f [98], g [93], h [45], i [15], j (present work)]. **d** Cyclic stability test of the AgNW/PNC strain sensor: 90 repetitive cycles of stretch to strain 80% then release back to strain of 0%

tains its electrical sensitivity at higher strains than those with higher gauge factors [45, 93–99]. While many self-healing polymers that obtain higher strain usually have lower gauge factors and lower sensing capabilities [100–102], the high gauge factor for the AgNW/PNC is significant due to an initial low resistance [87], increases during stretching [103], and matrix alignment [87, 103]. The increase in sensitivity is not due solely to the distance between AgNW's, instead, an increased number of junctions in the AgNW/PNC and an overall increase in the network density [103].

The results of a cyclic stretch-release test of the AgNW/PNC strain sensor are presented in Fig. 6d. By continuously monitoring the relative resistance change, two groups of values (at strain 0% and strain 80%) are very consistent without any noticeable shifts. The difference of relative resistance changes between each cycle is within 5% for all cycles. This demonstrates that the AgNW/PNC strain sensor has excellent mechanical and electrical stability and can be used for dynamic strain sensing without fear of hysteresis or drifting.

An important thing to note is that while many strain sensors can only produce the piezoelectric effect in one direction or when strained in one motion, the AgNW/PNC is omnidirectional. Figure 7 shows how the relative resistance of the sensor changes when twisted and flexed over various angles. The change in relative resistance relative to the flexion angle in Fig. 7b indicates that the relationship between relative resistance change and flexion angle is very linear for both the AgNW/PNC and for the polymer complex. This indicates that the sensor can reliably be used to predict, without calibration, what angle a finger (or any other joint on the

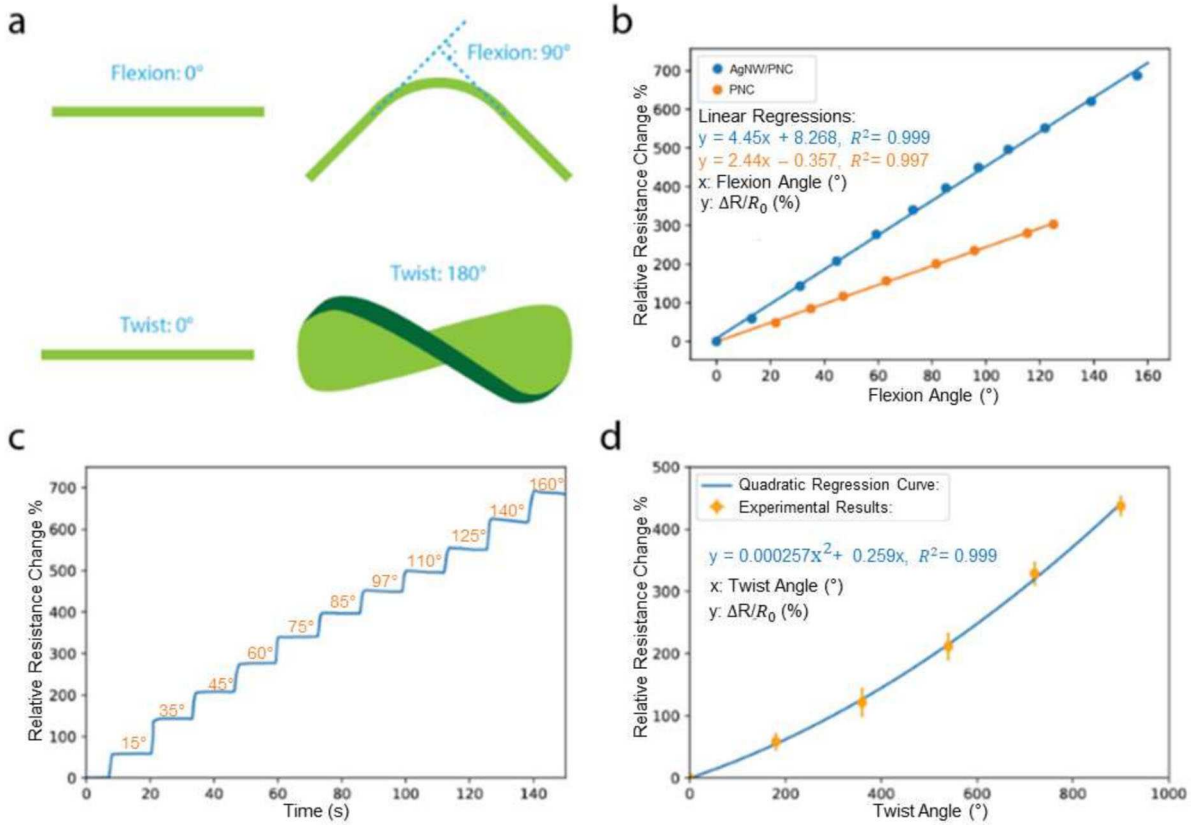

Fig. 7 Flexion bending. **a** Schematic diagram demonstrating the deformations of flexion bending and twisting. **b** The relationship of relative resistance changes versus flexion bending angles. (Polymer Complex: 0 to 125°, AgNW/PNC: 0 to 160°. **c** Plot of relative resistance change versus time for incremental flexion bending deformations. The time period for each bending angle is 13 s. **d** The relationship of relative resistance changes versus twisting angles from 0 to 900° for AgNW/PNC strain sensor

body, regardless of bending radius) has bent from 0 to 180°. The larger gauge factor and increase in sensitivity of the AgNW/PNC relative to the neat polymer complex correlates to a larger slope in Fig. 7b. Figure 7c illustrates that the relative resistance change is stable when bent and maintained at incremental angles. This signifies that over the course of 13 s, the sensor exhibits no relaxation phenomena, and the relative resistance will not drift. Figure 7d demonstrates that there is a quadratic relationship between twisting angles and relative resistance change. While many strain sensors may struggle to accurately detect twisting motions, the AgNW/PNC exhibits a high coefficient of determination value for the quadratic line equation, indicating that accurate changes in twist angle can still be found fairly easily utilizing the determined quadratic calibration curve. Being able to measure twist angles is imperative in numerous biomedical applications, the most obvious of which involve the radius and ulna.

For a polymer to be used in wearable sensors, it must possess comparable properties to the skin in terms of stretchability, elasticity, Young's modulus, and self-healing—being able to regain both mechanical and electronic properties with high efficiency. In order to be used in soft robots, these materials must have excellent stretchability (strain above 1000%), high toughness, high electrical conductivity, and low Young's modulus [104]. Self-healing properties are necessary to be resistant to internal and/or external mechanical damage caused by wear and tear, cuts, and rips [105]. Additionally, the conductive polymer materials must have excellent mechanical properties with high electrical conductivities for sensitive measurements or actuation that are reliable and repeatable, without drift over time. Unfortunately, the crystallinity required to transport charge carriers in polymers typically results in rigid molecular structures and thus tend to have poor mechanical properties [106, 107]. This leads to a low fracture resistance, making the polymer only slightly better than traditional inorganic alternatives. The AgNW/PNC complex, however, boasts excellent stretchability, high electrical sensitivity, self-healing ability, and a low Young's modulus. Compared to 9 other wearable sensors reported in the field, the AgNW/PNC is twice as stretchable as the next closest, while simultaneously exhibiting a gauge factor that is significantly higher than most other

available sensors, as seen in Fig. 7c. Additionally, the varied molecular structure and crystallinity of many organic materials result in irregular mechanical properties, making it difficult to use in a scalable manufacturing setting. It is desirable, then, for a stretchable electronic polymer material to be autonomously self-healing—without intervention, as well as robust, extremely sensitive, compliant to human skin for wearable applications, and easily scalable.

The AgNW/PNC can easily be fabricated into a wearable strain sensor thanks to its electrically conductive nature, self-healing ability, and ultrahigh stretchability. The electronic properties of the AgNW/PNC have unprecedented sensitivities to physical deformations despite the material being extremely soft and highly stretchable. This increase in sensitivity is likely not only a result of the conductivity increasing, but also a result of the bending, stretching, and twisting of the AgNW percolation network causing voids to form. In Fig. 7b, it can be seen that in both the PNC and AgNW/PNC, the conductivity of the material decreases with increased flexion angle. This is due to the flexion bending creating strain, where the displacement of conductive pathways within the polymer matrix causes the resistance to increase. When these materials undergo stretching such as they do during tensile testing, the same displacement and interruption of conductive pathways also increases the resistance of the material, thus lowering the conductivity. The reason that the relative resistance change of the AgNW/PNC is more sensitive with strain applied as a result of bending and/or stretching, however, is the easier interruption of the AgNW percolation networks and conductive pathways. When an individual nanowire experiences strain via the sensor being bent, twisted, or stretched, the polymer complex which had originally been cast around the AgNWs will no longer be perfectly flush and interconnected to those AgNWs. A microscopic void between the AgNW and the polymer complex will form. As a result, the AgNW percolation network will be susceptible to increases in electrical resistance, which will increase substantially relative to the resistance change one would see in the neat polymer complex under congruent strain.

As demonstrated by its gauge factor, the AgNW/PNC wearable sensor has an exceedingly high response to delicate perturbations such as pulse and speech-related vibrations. This allows it to be used for some fairly delicate applications. Figure 8a shows the AgNW/PNC wearable sensor successfully monitoring the carotid artery pulse of the wearer. Based on the monitored frequency, the heart rate of the wearer was found to be around 75 beats per minute which is consistent with the results tested by typical methods. The typical human pulse consists of three characteristic waves. The main wave or superior wave, the predicrotic wave, and the dicrotic wave can all be successfully recorded in a single pulse by the AgNW/PNC wearable sensor [108]. Figure 8b demonstrates the sensor's ability with regard to deep breathing (or diaphragmatic breathing). Based on the relative resistance change measured by the sensor, deep breathing will cause a significantly larger perturbation than the carotid artery pulse. The intensity of deep breathing is about 15 times that of the carotid artery pulse based on the monitored signal. The small waves on the right shoulder of the deep breathing peak are

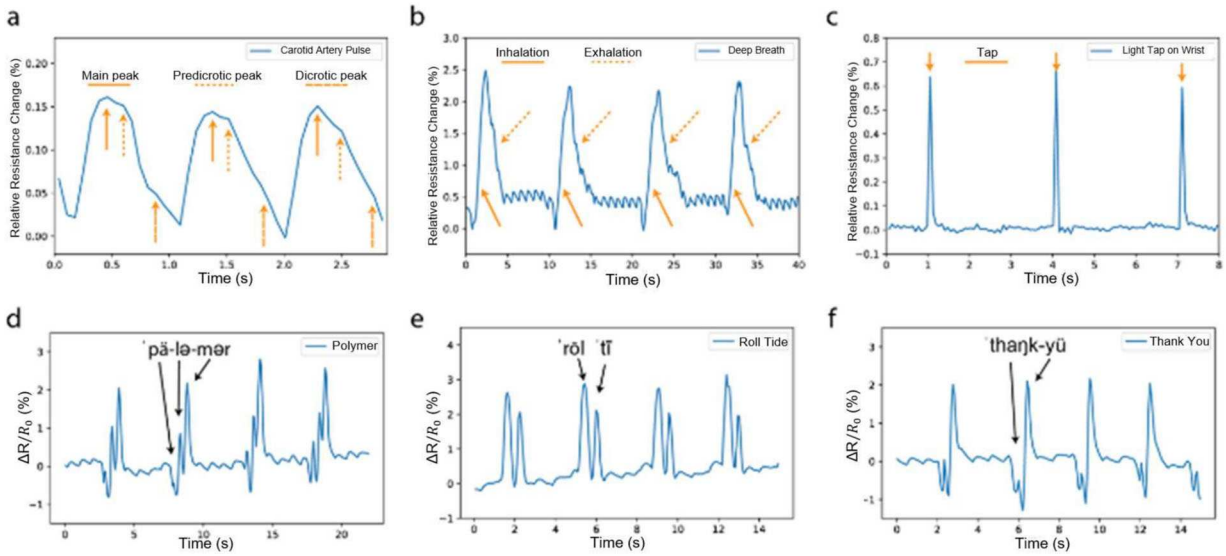

Fig. 8 Monitoring delicate motions in real time. **a** Relative resistance change in response to carotid artery pulse (sensor placed on the right upper side of the neck, just below the jaw). **b** Relative resistance changes in response to deep breath (sensor placed on the throat). **c** Relative resistance changes in response to light taps on wrist (sensor placed on the outer wrist). **d–f** Relative resistance change in response to speaking words of "Polymer," "Roll Tide," and "Thank You" (sensor placed on the throat) for speech recognition

believed to be the periodic pulse as well. Figure 8d-f shows that the sensor is capable of not only detecting vocal vibrations but is capable of differentiating various annunciations and words. This is exhibited as the wearer said "polymer," "roll tide," and "thank you." It can be seen that the change in relative resistance exhibited in the "polymer" pattern, "roll tide" pattern, and the "thank you" pattern all have different numbers of peaks, as well as peak sizes which can be used to differentiate them from one another.

To explore the lower limit of detection of the AgNW/PNC sensor, we show consistent changes in resistance for minute pressures over a range of 77 Pa to 390 Pa, as shown in Fig. S4. The relative resistance change at 390 Pa was around 2% when applied to the sensor, and the change at a pressure of 77 Pa is less than 0.01%. The results in Fig. S4 show a repeatable and consistent relative resistance change for several minute pressure cycles. This data indicates a linear relationship based on force, with a high coefficient of determination value of 0.97. The sensor's limit of quantification appears to be at approximately 200 Pa. Below this threshold the sensor no longer provides a linear response to the stimuli, meaning that while we may be able to still detect stimuli beneath this value, we would be unable to accurately quantify and predict it. The sensor can still reliably pick up perturbations down to 77 Pa, just without a linear response. The data also indicates that the sensors have a lower limit of detection of 0.0259 g/Pa. The sensor can, however, accurately differentiate pressures within the range of 200 Pa to 400 Pa by utilizing the linear relationship between those points.

The sensor also shows promise in applications as a topographical sensor. Figure 9 shows that the sensor is accurately able to pick up the general shape of an object using the piezoresistive effect that results from it being dragged over a 3-dimensional surface. When dragged perpendicularly across a 3-dimensional shape, the change in relative resistance as the sensor bends to glide across the surface can be measured. By doing multiple scans (in this case 4) of the sensor across the surface, we can plot the change in relative resistance for the entire outline of the shape. We can then normalize the data for each sweep, using the noiseless data as a baseline, thus converting this data into a topographical map. This demonstrates that the sensor can successfully scan and therefore identify shapes, lending itself to a variety of applications in soft robotics and prosthetics.

3 Conclusions

Nanofillers in the form of AgNWs were added to a newly developed polymer complex. The AgNW/PNC formed shows excellent mechanical properties, while being autonomously and rapidly self-healing, with a high GF and self-healing efficiency. The highly stable electronic properties of the AgNW/PNC, in conjunction with the high GF, allowed this to be applied to high-sensitivity force and vibration detection applications, including biomedical sensing (wearable motion, pulse, and speech monitoring) and e-skin topographical sensing. This piezoresistive polymer complex is significantly more stretchable than other ultra-stretchable sensors in the field at this time. [109–111]. It also boasts higher sensitivities than other AgNW-based composites [112, 113]. It is hypothesized that the superior mechanical properties were due to the increased connectivity, as a result of polymer chain pinning to the nanofiller, as shown by the rheological study. The rearrangement of the polymer complex in the presence of these AgNWs is thought to have accounted for the increase in sensitivity, as well. Additionally, these materials have been shown to be highly scalable and processable from a top-down or bottom-up route, with the added benefit of being compatible with 3D printing. With such robust stretchability as well as the ability to accurately sense strains as minute as vocal vibrations, the AgNW/PNC complex demonstrates great promise in applications such as stretchable/soft robotics and biomedical monitoring. In future work, an increase in conductivity will be targeted, to yield better electronic sensitivity while preserving the AgNW/PNC's unprecedented mechanical and self-healing properties.

4 Experimental Section

Materials: A 10 wt.% poly(2-acrylamido-2-methyl-1-propanesulfonic acid) (average molecular weight: 800,000) aqueous solution and 50 wt.% phytic acid aqueous solution were purchased from Acros Organics (Fair Lawn, NJ). Aniline (ACS grade) and ammonium persulfate (ACS grade) were purchased from Sigma-Aldrich (St. Louis, MO). Silver nanowires ethanol dispersion (concentration: 20 mg/mL, average diameter: 20 nm, average length: 20–30 μm) was obtained from ACS Materials (Pasadena, CA). All chemicals were used as received without further purification.

Preparation of polymer complex (PAAMPSA-PANI-PA) and AgNW/PNC: To solution cast the ternary polymer complex film, the polymer solution was prepared [15], as shown in Fig. 1. 10 wt.% PAAMPSA (50 g), PA (2.5 g), and monomer aniline (0.5 g) were mixed together. Then 3.2 g of 21.5 wt.% of APS aqueous solution was added into the mixture to initialize the in-situ oxidative polymerization of aniline. The reaction was maintained at 0°C in an ice-water bath for 3 h and at room temperature for the subsequent 21 h. The black free-standing polymer complex film was formed by drying at 35°C for 24 h. As for the AgNW/PNC, 2 mL of AgNWs were added after the polymerization of aniline completed. After the addition of the nanowires, the AgNW/PNC mixture suspension was magnetically stirred for 2 h, then sonicated in a water bath for an additional hour. The dark green

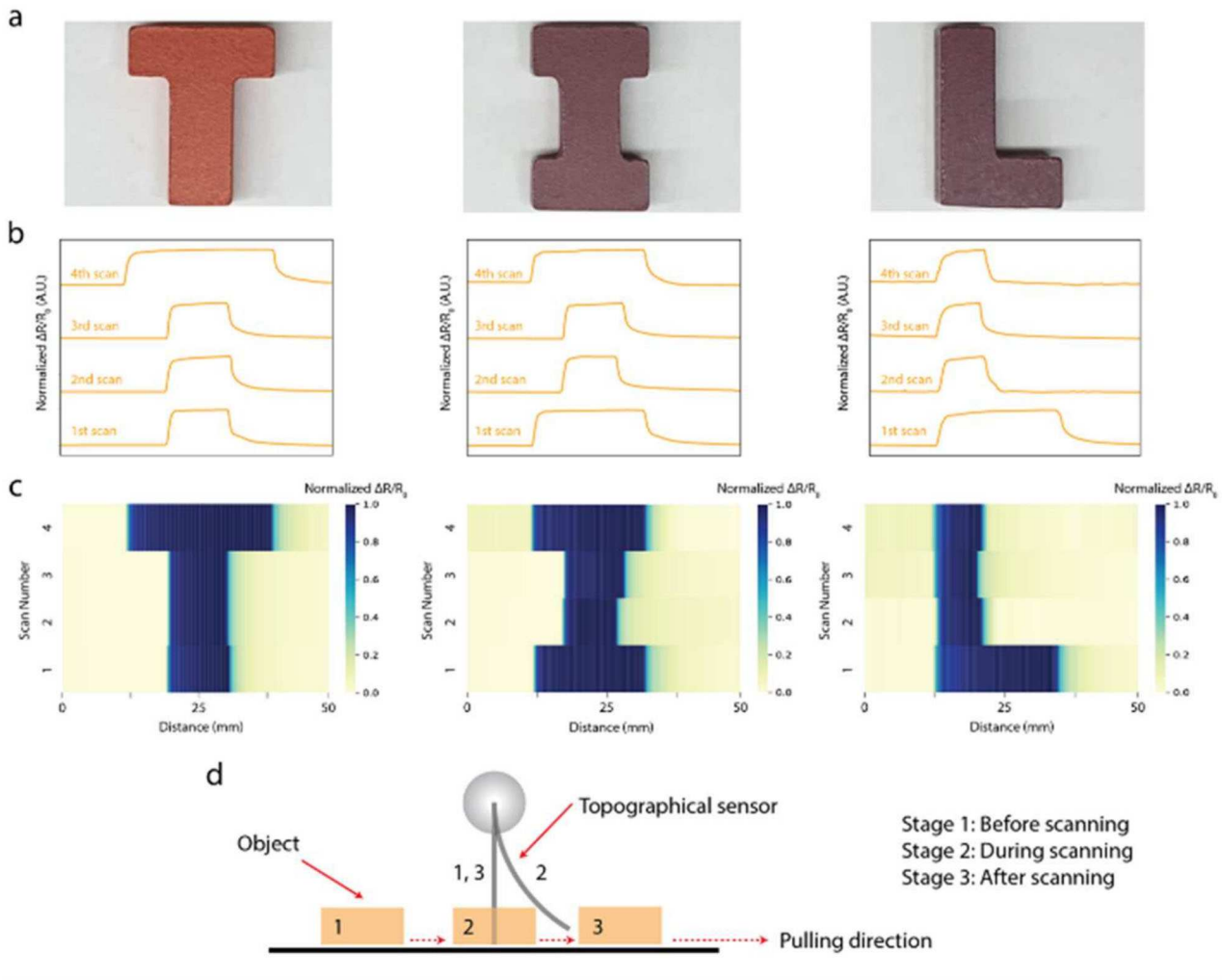

Fig. 9 AgNW/PNC nanocomposite as a topographical sensor. **a** The chosen objects to be scanned: wood alphabet letters "T," "I," and "L." The height of the letter objects are all 40 mm. **b** Four horizontal scans for each letter object by monitoring the electrical resistance. Each horizontal scan records a profile for a width of 10 mm and a length of 50 mm. The electrical resistance is normalized with a range of 0 to 1. **c** Heatmaps constructed by normalized resistance scans. **d** Schematic diagram of the AgNW/PNC topographical scanner

free-standing AgNW/PNC film was formed by the solution casting method as well. To allow for even dispersion of the AgNWs, the suspension was first dried at 50°C for 5 h, then at 35°C for 20 h.

Fabrication of AgNW/PNC strain sensor: To fabricate the AgNW/PNC strain sensor, the AgNW/PNC film was first cut into a rectangular shape (length: 40 mm, width: 10 mm, thickness: 0.9 mm). The electrical wires were connected at both longitudinal ends. The wired electrically conductive AgNW/PNC film was then sandwiched by a stretchable transparent acrylic adhesive tape (3 M, VHB Tape 4910). The adhesive tape acts as the encapsulant to prevent the film from contamination and provides additional elastic traction when the sensor is being stretched. The sandwiched strain sensor was left under ambient conditions for 24 h to achieve at least 90% of bond strength between the acrylic tape and AgNW/PNC. The polymer complex strain sensor was fabricated using the same procedure as the control.

Characterization of AgNW/PNC and polymer complex material: The chemical bonding of the materials was analyzed by the Fourier transform infrared spectroscopy (FT-IR, Fig. S1, PerkinElmer Spectrum Two) with a range between 500 to 4000 cm-1. Thermal gravimetric analysis (TGA) and differential scanning calorimetry analysis (DSC) (Fig. S2) were performed on a Simultaneous Thermal Analyzer 8000 (PerkinElmer Inc.) by heating from 30 to 820°C in an N2 atmosphere. The heating rate was set at 10°C/min. Scanning electron microscope (SEM, JEOL 7000 FE SEM) and energy-dispersive X-ray spectroscopy (EDS) mapping were employed to characterize the morphology and elemental composition of the materials. Testing samples were vacuum-dried for at least 24 h prior to imaging. X-ray photoelectron

spectroscopy (XPS, Fig. S3) was performed using a Kratos Axis DLD spectrometer with a monochromatic Al Kα radiation source (hν = 1486.6 eV). The binding energy of the core level C 1 s peak at 284.4 eV was used as a reference to exclude charging effects. Tensile tests were carried out on a universal tensile tester (MTS QTest 25). Testing films were fixed by pneumatic pressure (20 psi). The gauge length and the strain rate were set at 16 mm, and 40 mm/min, respectively.

Sensor evaluation: Electrical activity on the sensor was gathered using a Keithly (2450 Source Measure Unit). The self-healing tests involved cutting the polymer in half and then monitoring its relative resistance change for five cycles over the time span of 80 s. The electrical changes of the sensor were recorded using the (MTS QTest 25); and from this data, the Gauge factor and maximum resistance were calculated. Electrical activity was recorded for various bending angles from 0 to 900°, with the time span held for each angle being 13 s. The sensor was taped to a person's neck to monitor speech, pulse and breathing patterns. To test the effect of pressure (Fig. S4), various pressures were applied on the sensor , and the relative resistance was recorded over eight cycles. In order to do topographic scans, the sensor was dragged across objects horizontally while connected to the Keithly workstation. Various objects of 40 mm in height were scanned horizontally. Each scan is a length of 50 mm and a width of 10 mm. Heat maps were then constructed based on the scans.

Associated content

Supporting information

Supporting Information is available from the ACS website or from the author. Additional experiments, including FT-IR, TGA/DSC, XPS, and electronic data from the high-sensitivity pressure-based sensor analysis are found here in PDF format. This material is available free of charge via the Internet at http://pubs.acs.org.

Supplementary Information The online version contains supplementary material available at https://doi.org/10.1007/s42114-025-01361-7.

Acknowledgements The authors would like to thank the University of Maine, UM Maine College of Engineering and Computing, UM Department of Chemical and Biomedical Engineering, and UM Advanced Structures and Composites Center for experimental and characterization support.

Author contributions Conceptualization was carried out by Y.L., J.-W.J., and E.K.W. Validation and formal analysis were performed by Y.L., C.D., and E.K.W. Investigation was conducted by C.D., A.A. D.H., K.W., S.V., G.C., E.L., G.L., Z.L., and Y.L. Resources were provided by R.W., S.Y., Z.G., Z.F., and L.B. Writing of the original draft was conducted by C.D., Y.L., and E.K.W. Manuscripts review & editing was conducted by S.Y., Z.F., L.B., Y.L., J.-W.J., and E.K.W. Visualization was done by Y.L. and C.D. Supervision, project administration, and funding acquisition was conducted by E.K.W.

Funding E. Wujcik would like to acknowledge partial support from a National Science Foundation (NSF) CAREER Award from the Electronic/Photonic Materials program (NSF/MPS/DMR/EPM; award: 1942492), a Department of Defense (DoD) Air Force Office of Scientific Research (AFOSR) Air Force Research Laboratory (AFRL) Summer Faculty Fellowship (Materials and Manufacturing [RX]), as well as from a University of Alabama Office for Research and Economic Development (ORED) 2019 Research Grants Committee award (RG14899). Support for K. Webb was provided by a US National Science Foundation (NSF) Division of Engineering Education and Centers/ Directorate of Engineering Research Experience for Undergraduates (REU) Program (1851974).
Partial support for C. Duprey was provided by a Department of Education (DoEd) GAANN program (P200A180056), a Department of Defense (DoD) Air Force Office of Scientific Research (AFOSR) Air Force Research Laboratory (AFRL) Summer Fellowship (Materials and Manufacturing [RX]), and Department of Defense (DoD) U.S. Army Natick Soldier Systems Center grants (awards: W911QY-18-C-0101 and W911QY-20-C-0053).
Visiting Scholar support for D. Hong was provided by Kookmin University.

Data Availability No datasets were generated or analysed during the current study.

Declarations

Competing Interests The authors declare no competing interests.

References

1. Jafarian H, Dadashi Firouzjaei M, Aghapour Aktij S, Aghaei A, Pilevar Khomami M, Elliott M, Wujcik EK, Sadrzadeh M, Rahimpour A (2023) Synthesis of heterogeneous metal organic framework-graphene oxide nanocomposite membranes for water treatment. Chem Eng J 455:140851
2. Dadashi Firouzjaei M, Zolghadr E, Arabi Shamsabadi A, Sadrzadeh M, Rahimpour A, Akbari Afkhami F, Wujcik EK, Elliott M (2023) Clean water recycling through adsorption via heterogeneous nanocomposites: silver-based metal-organic framework embellished with graphene oxide and MXene. Case Stud Chem Environ Eng 7:100296

3. Uddin MN, Le L, Nair R, Asmatulu R (2019) Effects of graphene oxide thin films and nanocomposite coatings on flame retardancy and thermal stability of aircraft composites: a comparative study. J Eng Mater Technol 141(3):031004
4. Li Z, Chen S, Nambiar S, Sun Y, Zhang M, Zheng W, Yeow JTW (2016) PMMA/MWCNT nanocomposite for proton radiation shielding applications. Nanotechnology 27(23):234001
5. Dash K, Chaira D, Ray BC (2015) Microstructural evolution and sliding wear studies of copper-alumina micro- and nanocomposites fabricated by spark plasma sintering. J Mech Behav Mater 24(1–2):25–34
6. Huang X, Jiang P (2015) Core-shell structured high- k polymer nanocomposites for energy storage and dielectric applications. Adv Mater 27(3):546–554
7. Siwal SS, Zhang Q, Devi N, Thakur VK (2020) Carbon-based polymer nanocomposite for high-performance energy storage applications. Polymers 12(3):505
8. Taha T, Mahmoud M (2021) Synthesis and characterization of PVDF-Er2O3 polymer nanocomposites for energy storage applications. Mater Chem Phys 270:124827
9. Blasdel NJ, Wujcik EK, Carletta JE, Lee KS, Monty CN (2015) Fabric nanocomposite resistance temperature detector. IEEE Sens J 15(1):300–306
10. Wujcik EK, Blasdel NJ, Trowbridge D, Monty CN (2013) Ion sensor for the quantification of sodium in sweat samples. IEEE Sens J 13(9):3430–3436
11. Heikenfeld J, Jajack A, Rogers J et al (2018) Wearable sensors: modalities, challenges, and prospects. Lab Chip 18(2):217–248
12. Horne J, McLoughlin L, Bridgers B, Wujcik EK (2020) Recent developments in nanofiber-based sensors for disease detection, immunosensing, and monitoring. Sens Actuat Rep 2:100005
13. Lu Y, Biswas MC, Guo Z, Jeon J-W, Wujcik EK (2019) Recent developments in bio-monitoring via advanced polymer nanocomposite-based wearable strain sensors. Biosens Bioelectron 123:167–177
14. Horne J, McLoughlin L, Bury E, Koh AS, Wujcik EK (2020) Interfacial phenomena of advanced composite materials toward wearable platforms for biological and environmental monitoring sensors, armor, and soft robotics. Adv Mater Interfaces 7:1901851
15. Lu Y, Liu Z, Yan H, Peng Q, Wang R, Barkey ME, Jeon JW, Wujcik EK (2019) Ultrastretchable conductive polymer complex as a strain sensor with a repeatable autonomous self-healing ability. ACS Appl Mater Interf 11:20453–20464
16. Hu RH, Ji G, Wang Y, Zhao J, Zheng J (2021) Rational design of multiple hydrogen bonds to improve the mechanical property of rigid PANI. Extr Mech Lett 42
17. Ibrahim KA (2017) Synthesis and characterization of polyaniline and poly(aniline-co-o-nitroaniline) using vibrational spectroscopy. Arab J Chem 10:S2668–S2674
18. Wujcik EK, Jeon JW, Lu Y. Self-healing and stretchable polymeric compositions. U.S. Patent
19. Zeraati AS, Arjmand M, Sundararaj U (2017) Silver nanowire/MnO. ACS Appl Mat Interf 9:14328–14336
20. Wang S, Tian Y, Hang C, Wang C (2018) Cohesively enhanced electrical conductivity and thermal stability of silver nanowire networks by nickel ion bridge joining. Sci Rep 8:5260
21. Zhang D, Sun H, Huang M, Su M, Ma Y, Shi M, Mi L, Liu C, Liu H (2024) Construction of “island-bridge" microstructured conductive coating for enhanced impedance response of organohydrogel strain sensor. Chem Eng J 496:153752
22. Tian Y, Huang M, Wang Y, Zheng Y, Yin R, Liu H, Liu C, Shen C (2024) Ultra-stretchable, sensitive and breathable electronic skin based on TPU electrospinning fibrous membrane with microcrack structure for human motion monitoring and self-powered application. Chem Eng J 480:147899
23. Yang S, Yang W, Yin R, Liu H, Sun H, Pan C, Liu C, Shen C (2023) Waterproof conductive fiber with microcracked synergistic conductive layer for high-performance tunable wearable strain sensor. Chem Eng J 453:139716
24. Fang Q (2021) Lafdi, K. Effect of nanofiller morphology on the electrical conductivity of polymer nanocomposites. Nano Express 2
25. Tang X, Peng L, Shi S, Fu M (2019) Influence of crystal structure on size dependent deformation behavior and strain heterogeneity in micro-scale deformation. Inter J Plasticit 118
26. Huang H, Cai CJ, Yeow BS, Ouyang J, Ren H (2021) Highly stretchable and Kirigami-structured strain sensors with long silver nanowires of high aspect ratio. Machines 9:186
27. Li W, Meredov A, Shamim A (2019) Coat-and-print patterning of silver nanowires for flexible and transparent electronics. npj Flexib Electron 3:19
28. Balazs AC (2007) Modeling self-healing materials. Mater Today 10:18–23
29. Kratz K, Narasimhan A, Tangirala R, Moon S, Revanur R, Kundu S, Kim HS, Crosby AJ, Russell TP, Emrick T, Kolmakov G, Balazs AC (2012) Probing and repairing damaged surfaces with nanoparticle-containing microcapsules. Nat Nanotechnol 7:87–90
30. Monty C, Wujcik E, Blasdel N (2017) Flexible electrode for detecting changes in temperature, humidity, and sodium ion concentration in sweat. U.S. Patent, US 9,603,560 B2
31. Marín-Morales J, Higuera-Trujillo JL, Greco A, Guixeres J, Llinares C, Scilingo EP, Alca niz M, Valenza G (2018) Affective computing in virtual reality: emotion recognition from brain and heartbeat dynamics using wearable sensors. Scientif Rep 8:13657
32. Baumgartner M et al (2020) Resilient yet entirely degradable gelatin-based biogels for soft robots and electronics. Nat Mater 19:1102–1109
33. Zhan CX, Yu GQ, Lu Y, Wang LY, Wujcik E, Wei SY (2017) Conductive polymer nanocomposites: a critical review of modern advanced devices. J Mater Chem C 5:1569–1585
34. Ma Y, Ma M, Yin X, Shao Q, Lu N, Feng Y, Lu Y, Wujcik EK, Mai X, Wang C, Guo Z (2018) Tuning polyaniline nanostructures via end group substitutions and their morphology dependent electrochemical performances. Polymer 156:128–135
35. Zhai L, Narkar A, Ahn K (2020) Self-healing polymers with nanomaterials and nanostructures. Nano Today 30
36. Hornat CC, Urban MW (2020) Shape memory effects in self-healing polymers. Progress in Polymer Sci 102
37. Hager MD, Greil P, Leyens C, van der Zwaag S, Schubert US (2010) Self-healing materials. Advanded Materials 22:5424–30
38. Zechel S, Geitner R, Abend M, Siegmann M, Enke M, Kuhl N, Klein M, Vitz J, Gräfe S, Dietzek B et al (2017) Intrinsic self-healing polymers with a high E-modulus based on dynamic reversible urea bonds. NPG Asia Materials 9:e420–e420
39. Blaiszik B, Kramer S, Olugebefola S, Moore J, Sottos N (2010) Self-healing polymers and composites. Annual Rev Mat Res 40
40. Guo H, Han Y, Zhao W, Yang J, Zhang L (2020) Universally autonomous self-healing elastomer with high stretchability. Nat Commun 11:2037
41. Shin S-H, Kim S-M, Jeon H, Hwang SY, Oh DX, Park J (2020) Skin-inspired hydrogel-elastomer hybrid forms a seamless interface by autonomous hetero-self-healing. ACS Appl Polym Mat 2:5352–5357
42. Utrera-Barrios S, Hernández Santana M, Verdejo R, López-Manchado MA (2020) Design of rubber composites with autonomous self-healing capability. ACS Omega 5:1902–1910
43. Urban MW, Davydovich D, Yang Y, Demir T, Zhang Y, Casabianca L (2018) Key-and-lock commodity self-healing copolymers. Science 362:220–225

44. Thangavel G, Tan MWM, Lee PS (2019) Advances in self-healing supramolecular soft materials and nanocomposites. Nano Converg 6:29–29
45. Zhang L, Li H, Lai X, Gao T, Zeng X (2020) Three-dimensional binary-conductive-network silver nanowires@thiolated graphene foam-based room-temperature self-healable strain sensor for human motion detection. ACS Appl Mater Interf 12:44360–44370
46. Zhang L, Liu Z, Wu X, Guan Q, Chen S, Sun L, Guo Y, Wang S, Song J, Jeffries EM, He C, Qing FL, Bao X, You Z (2019) A highly efficient self-healing elastomer with unprecedented mechanical properties. Adv Mater 31:e1901402
47. Sapurina I, Shishov M (2012) In new polymers for special applications; De Souza Gomes, A., Ed.; InTech
48. Sapurina I, Stejskal J (2008) The mechanism of the oxidative polymerization of aniline and the formation of supramolecular polyaniline structures. Polym Int 57:1295–1325
49. Ma Z, Shi W, Yan K, Pan L, Yu G (2019) Doping engineering of conductive polymer hydrogels and their application in advanced sensor technologies. Chem Sci 10:6232–6244
50. Guo Y, Bae J, Zhao F, Yu G (2019) Functional hydrogels for next-generation batteries and supercapacitors. Trends in Chemistry 1
51. Ballabio M, Zhang T, Chen C, Zhang P, Liao Z, Hambsch M, Mannsfeld SCB, Zschech E, Sirringhaus H, Feng X, Bonn M, Dong R, Cánovas E (2021) Band-like charge transport in phytic acid-doped polyaniline thin films. Adv Funct Mat n/a, 2105184
52. Ji J, Li R, Li H, Shu Y, Li Y, Qiu S, He C, Yang Y (2018) Phytic acid assisted fabrication of graphene/polyaniline composite hydrogels for high-capacitance supercapacitors. Compos B Eng 155:132–137
53. Yoo J, Bae, J (2013) The influence of aniline to acid composition on the electrical conductivity of PANI-PAAMPSA. Bullet Korean Chem Soc 34
54. Son D et al (2018) An integrated self-healable electronic skin system fabricated via dynamic reconstruction of a nanostructured conducting network. Nat Nanotechnol
55. Choi S, Han SI, Jung D, Hwang HJ, Lim C, Bae S, Park OK, Tschabrunn CM, Lee M, Bae SY et al (2018) Highly conductive, stretchable and biocompatible Ag-Au core-sheath nanowire composite for wearable and implantable bioelectronics. Nat Nanotechnol 13:1048–1056
56. Frutiger A, Muth JT, Vogt DM, Mengüç Y, Campo A, Valentine AD, Walsh CJ, Lewis JA (2015) Capacitive soft strain sensors via multicore-shell fiber printing. Adv Mater 27:2440–2446
57. Cummings J, Lowengrub JS, Sumpter BG, Wise SM, Kumar R (2018) Modeling solvent evaporation during thin film formation in phase separating polymer mixtures. Soft Matter 14:1833–1846
58. Mohammadpour-Haratbar A, Zare Y, Rhee KY (2023) Simulation of electrical conductivity for polymer silver nanowires systems. Sci Rep 13:5
59. Boey JY, Lee CK, Tay GS (2022) Factors affecting mechanical properties of reinforced bioplastics: a review. Polymers 14:3737
60. Park B, Ryu Y, Yong K (2004) Growth and characterization of silicon carbide nanowires. Surf Rev Lett 11:373–378
61. Wang D-H, Xu D, Wang Q, Hao Y-J, Jin G-Q, Guo X-Y, Tu KN (2008) Periodically twinned SiC nanowires. Nanotechnology 19:215602
62. Chen Y, Zhang C, Li L, Zhou S, Chen X, Gao J, Zhao N, Wong C (2019) Hybrid anodic and metal-assisted chemical etching method enabling fabrication of silicon carbide nanowires. Small 15:1803898
63. Kar K (2022) Handbook of fly ash; Elsevier
64. Song K (2017) Progress in rubber nanocomposites; Elsevier, pp 115–152
65. Su C-H, Chen H-L, Ju S-P, Chen H-Y, Shih C-W, Pan C-T, You T-D (2020) The mechanical behaviors of polyethylene/silver nanoparticle composites: an insight from molecular dynamics study. Sci Rep 10:7600
66. De Almeida SFM, Neto ZDSN (1994) Effect of void content on the strength of composite laminates. Compos Struct 28:139–148
67. Hyde A, He J, Cui X, Lua J, Liu L (2020) Effects of microvoids on strength of unidirectional fiber-reinforced composite materials. Compos B Eng 187:107844
68. Reddy CV (2017) Study of voids effect on tensile strength of carbon fiber reinforced composites for structural applications. Int J Res Appl Sci Eng Technol V, 1311–1320
69. Srolovitz D, Maeda K, Vitek V, Egami T (1981) Structural defects in amorphous solids Statistical analysis of a computer model. Philos Mag A 44:847–866
70. Zeng X, Zhou B, Gao Y, Wang C, Li S, Yeung CY, Wen W (2014) Structural dependence of silver nanowires on polyvinyl pyrrolidone (PVP) chain length. Nanotechnology 25:495601
71. Sides SW, Grest GS, Stevens MJ (2002) Large-scale simulation of adhesion dynamics for end-grafted polymers. Macromolecules 35:566–573
72. Souri H, Banerjee H, Jusufi A, Radacsi N, Stokes AA, Park I, Sitti M, Amjadi M (2020) Wearable and stretchable strain sensors: materials, sensing mechanisms, and applications. Adv Intell Syst 2:2000039
73. Sun H, Dai K, Zhai W, Zhou Y, Li J, Zheng G, Li B, Liu C, Shen C (2019) A highly sensitive and stretchable yarn strain sensor for human motion tracking utilizing a wrinkle-assisted crack structure. ACS Appl Mat Interf 11:36052–36062
74. Xu M, Qi J, Li F, Zhang Y (2018) Highly stretchable strain sensors with reduced graphene oxide sensing liquids for wearable electronics. Nanoscale 10:5264–5271
75. Shi G, Zhao Z, Pai J-H, Lee I, Zhang L, Stevenson C, Ishara K, Zhang R, Zhu H, Ma J (2016) Highly sensitive, wearable, durable strain sensors and stretchable conductors using graphene/silicon rubber composites. Adv Func Mater 26:7614–7625
76. Cao Z, Wang R, He T, Xu F, Sun J (2018) Interface-controlled conductive fibers for wearable strain sensors and stretchable conducting wires. ACS Appl Mater Interfaces 10:14087–14096
77. Cai Y, Shen J, Dai Z, Zang X, Dong Q, Guan G, Li L-J, Huang W, Dong X (2017) Extraordinarily stretchable all-carbon collaborative nanoarchitectures for epidermal sensors. Adv Mater 29:1606411
78. Bauer F, Denneler S, Willert-Porada M (2005) Influence of temperature and humidity on the mechanical properties of Nafion®117 polymer electrolyte membrane. J Polym Sci, Part B: Polym Phys 43:786–795
79. Liang X, Boppart SA (2010) Biomechanical properties of in vivo human skin from dynamic optical coherence elastography. IEEE Trans Biomed Eng 57:953–9
80. Sharma S, Rawal J, Dhakate SR, Singh BP (2020) Synergistic bridging effects of graphene oxide and carbon nanotube on mechanical properties of aramid fiber reinforced polycarbonate composite tape. Compos Sci Technol 199:108370
81. Shahdan D, Chen RS, Ahmad S (2021) Optimization of graphene nanoplatelets dispersion and nano-filler loading in bio-based polymer nanocomposites based on tensile and thermogravimetry analysis. J Market Res 15:1284–1299
82. Patterson BA, Malakooti MH, Lin J, Okorom A, Sodano HA (2018) Aramid nanofibers for multiscale fiber reinforcement of polymer composites. Compos Sci Technol 161:92–99
83. Yetgin SH (2019) Effect of multi walled carbon nanotube on mechanical, thermal and rheological properties of polypropylene. J Market Res 8:4725–4735
84. De Gennes P (1987) Polymers at an interface; a simplified view. Adv Coll Interface Sci 27:189–209
85. Napper DH (1989) Polymeric stabilization of colloidal dispersions, 3rd edn. Colloid science; Academic Press, London

86. Yue X, Fang C, Yao Q, Liu C, Shen C, Liu H (2024) Tunable porous fiber-shaped strain sensor with synergistic conductive network for human motion recognition and tactile sensing. Chem Eng J 491:151853
87. Shengbo S, Lihua L, Aoqun J, Qianqian D, Jianlong J, Qiang Z, Wendong Z (2018) Highly sensitive wearable strain sensor based on silver nanowires and nanoparticles. Nanotechnology 29:255202
88. Kotresh S, Ravikiran Y, Raj Prakash H, Vijaya Kumari S (2016) Polyaniline-titanium dioxide composite as humidity sensor at room temperature. Nanosystems: Phys Chem Math 732–739
89. Vlazan P, Ursu DH, Irina-Moisescu C, Miron I, Sfirloaga P, Rusu E (2015) Structural and electrical properties of TiO2/ZnO core-shell nanoparticles synthesized by hydrothermal method. Mater Charact 101:153–158
90. Lin W-D, Chang H-M, Wu R-J (2013) Applied novel sensing material graphene/polypyrrole for humidity sensor. Sens Actuators, B Chem 181:326–331
91. Lee CH, Khalina A, Lee SH (2021) Importance of interfacial adhesion condition on characterization of plant-fiber-reinforced polymer composites: a review. Polymers 13:438
92. Cai G, Wang J, Qian K, Chen J, Li S, Lee PS (2017) Extremely stretchable strain sensors based on conductive self-healing dynamic cross-links hydrogels for human-motion detection. Adv Sci 4:1600190
93. Ding J, Qiao Z, Zhang Y, Wei D, Chen S, Tang J, Chen L, Wei D, Sun J, Fan H (2020) NIR-responsive multi-healing HMPAM/dextran/AgNWs hydrogel sensor with recoverable mechanics and conductivity for human-machine interaction. Carbohyd Polym 247:116686
94. Glier TE, Betker M, Witte M, Matsuyama T, Westphal L, Grimm-Lebsanft B, Biebl F, Akinsinde LO, Fischer F, Rübhausen M (2020) Electrical and network properties of flexible silver-nanowire composite electrodes under mechanical strain. Nanoscale 12:23831–23837
95. Zhang S, Liu H, Yang S, Shi X, Zhang D, Shan C, Mi L, Liu C, Shen C, Guo Z (2019) Ultrasensitive and highly compressible piezoresistive sensor based on polyurethane sponge coated with a cracked cellulose nanofibril/silver nanowire layer. ACS Appl Mat Interf 11:10922–10932
96. Zhu GJ, Ren PG, Guo H, Jin YL, Yan DX, Li ZM (2019) Highly sensitive and stretchable polyurethane fiber strain sensors with embedded silver nanowires. ACS Appl Mat Interf 11:23649–23658
97. Li Y, Liu C, Lv X, Sun S (2021) A highly sensitive strain sensor based on a silica@polyaniline core-shell particle reinforced hydrogel with excellent exibility, stretchability, toughness and conductivity. Soft Matter 17:2142–2150
98. Jiao Y, Lu Y, Lu K, Yue Y, Xu X, Xiao H, Li J, Han J (2021) Highly stretchable and self-healing cellulose nanofiber-mediated conductive hydrogel towards strain sensing application. J Colloid Interface Sci 597:171–181
99. Jing X, Mi H-Y, Peng X-F, Turng L-S (2018) Biocompatible, self-healing, highly stretchable polyacrylic acid/reduced graphene oxide nanocomposite hydrogel sensors via mussel-inspired chemistry. Carbon 136:63–72
100. Dai X, Huang L-B, Du Y, Han J, Kong J (2021) Self-healing exible strain sensors based on dynamically cross-linked conductive nanocomposites. Composites Commun 24:100654
101. Chen J, Peng Q, Thundat T, Zeng H (2019) Stretchable, injectable, and self-healing conductive hydrogel enabled by multiple hydrogen bonding toward wearable electronics. Chem Mater 31:4553–4563
102. Rao VK, Shauloff N, Sui X, Wagner HD, Jelinek R (2020) Polydiacetylene hydrogel self-healing capacitive strain sensor. J Mater Chem C 8:6034–6041
103. Boland CS, Khan U, Benameur H, Coleman JN (2017) Surface coatings of silver nanowires lead to effective, high conductivity, high-strain, ultrathin sensors. Nanoscale 9:18507–18515
104. Lee Y, Song WJ, Sun JY (2020) Hydrogel soft robotics. Materials Today. Physics 15:100258
105. Kang J, Jeffrey B, Bao Z (2019) Self-healing soft electronics. Nat Electron 144–150
106. Dakovic M, Borovina M, Pisavicic M, Aakeroy CB, Soldin Z, Kukovec B-M, Kodrin I (2018) Mechanically responsive crystalline coordination polymers with controllable elasticity. Angew Chem Int Ed 57:14801–14805
107. Kim WK, Ma BS, Kim YH, Kim T-S (2021) Mechanical properties of organic semiconductors for flexible electronics. Organ Flexib Electron 199–223
108. Yao Y, Hao L, Xu L, Zhang Y, Qi L, Sun Y, Yang B, van de Vosse FN, Yao Y (2017) Diastolic augmentation index improves radial augmentation index in assessing arterial stiffness. Sci Rep 7:5864
109. Xu H, Lv Y, Qiu D, Zhou Y, Zeng H, Chu Y (2019) An ultra-stretchable, highly sensitive and biocompatible capacitive strain sensor from an ionic nanocomposite for on-skin monitoring. Nanoscale 11:1570–1578
110. Mai H, Mutlu R, Tawk C, Alici G, Sencadas V (2019) Ultra-stretchable MWCNT-Ecoflex piezoresistive sensors for human motion detection applications. Compos Sci Technol 173:118–124
111. Pandey D, Singh R, Karmakar P, Das S, Roy H, Sen S, Mandal S, Chanda N (2024) Monolithic MWCNT-hyperelastic elastomer based electronic skin with ultra-high stretchability for human health monitoring. Sens Actuators, A 372:115341
112. Wang J, Yue X, Li X, Dong J, Zhang Q, Zhao X (2022) Lightweight and elastic silver nanowire/PEDOT: PSS/polyimide aerogels for piezoresistive sensors. ACS Appl Polym Mater 4:3205–3216
113. Liu WC, Watt AA (2021) Solvodynamically printed silver nanowire/ethylene-co-vinyl acetate composite films as sensitive piezoresistive pressure sensors. ACS Appl Nano Mater 4:7905–7916

Authors and Affiliations

Colton Duprey[1,2] · Arya Ajeev[1] · Dajung Hong[3] · Katherine Webb[4] · Sarah Veres[5] · George Chen[5] · Emily Linn[5] · Gina Lusvardi[5] · Zhongqi Liu[6] · Ruigang Wang[6] · Sanggyu Yim[3] · Zhanhu Guo[7] · Zachary Farrell[8] · Luke A. Baldwin[9] · Yang Lu[10] · Ju-Won Jeon[3] · Evan K. Wujcik[1,2]

✉ Yang Lu
ylu635@gatech.edu

✉ Ju-Won Jeon
jwjeon@kookmin.ac.kr

✉ Evan K. Wujcik
Evan.Wujcik@maine.edu

[1] Materials Engineering And Nanosensor [MEAN] Laboratory, Department of Chemical and Biomedical Engineering, The University of Maine, Orono, ME 04469-5737, USA

[2] Advanced Structures and Composites Center [ASCC], The University of Maine, Orono, ME 04469-5793, USA

[3] Department of Chemistry, Kookmin University, Seoul 02707, Republic of Korea

[4] J. Crayton Pruitt Department of Biomedical Engineering, University of Florida, Gainsville, FL 32611, USA

[5] Department of Chemical and Biological Engineering, The University of Alabama, Tuscaloosa, AL 35487, USA

[6] Department of Metallurgical and Materials Engineering, The University of Alabama, Tuscaloosa, AL 35487, USA

[7] Department of Mechanical and Construction Engineering, Northumbria University, Newcastle upon Tyne, UK

[8] Cornerstone Research Group, Inc, Miamisburg, OH 45342, USA

[9] Materials and Manufacturing Directorate, Air Force Research Laboratory, Wright-Patterson AFB, Dayton, OH 45433, USA

[10] School of Chemical and Biomolecular Engineering, Georgia Institute of Technology, Atlanta, GA 30332, USA